

A comparison between Boussinesq and non-Boussinesq approximations for numerical simulation of natural convection in an annulus cavity

P. Mayeli and G.J. Sheard

The Sheard Lab, Department of Mechanical and Aerospace Engineering, Monash University, Melbourne, VIC 3800, Australia.

Abstract

Traditionally, the Boussinesq approximation is adopted for numerical simulation of natural convection phenomena where density variations are supposed negligible except through the gravity term of the momentum equation. In this study, a rather new formulation based on a non-Boussinesq approximation is presented in which the density variations are also considered in advection terms. The results of the proposed formulation is compared against Boussinesq simulation in a concentric horizontal annulus cavity in terms of average and local Nusselt number up to $Ra = 10^5$. Results indicate that the classic Boussinesq approximation works accurately up to $Ra = 10^4$ but at $Ra = 10^5$ computed thermo-fluid parameters via the two approaches are not identical.

Introduction

Numerical simulation of natural convection phenomena, due to their many scientific and technical applications such as solar collectors, foundry devices, geophysical and astrophysical processes, etc., has attracted attention of researchers during recent decades. Predicting the exact behaviour of such systems when natural convection is the dominant heat transfer mechanism is of paramount importance. Typically, the Boussinesq approximation (i.e. ignoring density variations except where they are multiplied by acceleration of the gravity [1]) is adopted for numerical simulation of natural convection problems. In this approach, often a linear simplification is applied that relates density and temperature variations via a volumetric thermal expansion coefficient.

The horizontal annulus cavity is a widely used benchmark problem in numerical heat transfer research. At low Rayleigh numbers (Ra), diffusion is the dominant mechanism, but as convection dominates the heat transfer mechanism at high Rayleigh numbers a thin boundary layer is formed along the solid boundaries, which presents a great challenge for any numerical method. This problem is solved by different numerical methods [2-6]. A steady state solution up to $Ra = 10^5$ is reported for this problem [3-6].

In all of the aforementioned works, it is supposed that the density variations are small so their effect is confined to the buoyancy term. This allows the flow field to be treated as incompressible. Note that in different situations, where the density varies under the influence of temperature non-uniformities are significant, the classical Boussinesq approximation may produce inaccurate results. In order to avoid applying the Boussinesq approximation in numerical simulation of natural convection problems there are three major remedies: The first is inserting the Gay-Lussac dimensionless number definition into the governing equations. This number describes the level of density variations caused by the temperature field. It may be shown that the Boussinesq approximation is retrieved as the Gay-Lussac number goes to zero [7]. For this approach, the difference of adopting Boussinesq approximation and inserting the Gay-Lussac

number to the computations for the Boussinesq regime, i.e. the threshold of the Rayleigh number that leads to a steady state solution, is studied by Szewc et al. [7] for a rectangular cavity filled with air with $Pr = 0.71$. They reported a 4% discrepancy of the average Nusselt number between the two approaches. The second remedy is considering density variations in all terms and inserting the concept of compressibility and Mach number in the computations. This task is performed by Vierendeels et al. [8] for numerical simulation of natural convection at low Mach number. Finally, the third remedy is considering density variations through the advection terms as well as the buoyancy term. This approach is proposed by Lopez et al. [9] both for inertial and rotating reference frames. They applied their formulation for numerical simulation of fluid flow confined between two differentially heated and rotating cylinders.

In this study, the approach of Lopez et al. [9] is adopted to produce a new form of the governing equations and is presented based on the idea of considering density variations through the advection term as well as the buoyancy term in momentum equations for natural convection problems. This formulation is implemented into an element-based finite volume method solver and its results are investigated for local and average Nusselt number in a horizontal concentric annulus cavity up to $Ra = 10^5$.

Governing equations

Under the Boussinesq approximation for buoyancy, density differences are neglected except with respect to the gravity term. In the present formulation, buoyancy effects are also considered with respect to the advection term. The steady-state incompressible momentum equation in vector form is expressed as

$$\rho(\mathbf{u} \cdot \nabla)\mathbf{u} = -\nabla p + \mu \nabla^2 \mathbf{u} + \rho g \mathbf{e}_g \quad (1)$$

Dividing Eq. (1) by reference density, ρ_0 , yields

$$\frac{\rho}{\rho_0}(\mathbf{u} \cdot \nabla)\mathbf{u} = -\frac{1}{\rho_0} \nabla p + \nu \nabla^2 \mathbf{u} + \frac{\rho}{\rho_0} g \mathbf{e}_g \quad (2)$$

Substituting the density state relation $\rho/\rho_0 = 1 - \beta\theta$ and a modified pressure $p^* = p - \rho_0\phi$ into the above equation yields

$$(\mathbf{u} \cdot \nabla)\mathbf{u} = -\frac{1}{\rho_0} \nabla p^* + \nu \nabla^2 \mathbf{u} - \beta\theta g \mathbf{e}_g + \beta\theta(\mathbf{u} \cdot \nabla)\mathbf{u} \quad (3)$$

Here ϕ is the gravitational potential whose gradient yields the gravitational acceleration vector i.e. $\nabla\phi = g\mathbf{e}_g$. Using the dimensionless parameters

$$X = \frac{x}{L}, Y = \frac{y}{L}, \tilde{r} = \frac{r - r_i}{r_o - r_i}, U = \frac{uL}{\alpha} \quad (4)$$

$$P = \frac{p^* L^2}{\rho \alpha^2}, \Theta = \frac{\theta}{\Delta\theta}$$

one can derive the dimensionless form of the momentum equation for natural convection problems,

$$(\mathbf{U} \cdot \nabla)\mathbf{U} = -\nabla P + Pr \nabla^2 \mathbf{U} - Ra Pr \theta \mathbf{e}_g + \beta \Delta \theta (\mathbf{U} \cdot \nabla)\mathbf{U}. \quad (5)$$

Here, the Prandtl number and Rayleigh number are defined as $Pr = \nu/\alpha$ and $Ra = g\beta\Delta\theta L_{ref}^3/\nu\alpha$, respectively. Introducing a dimensionless parameter characterising the square of the ratio of thermal diffusivity to gravitational effects as $\gamma = \alpha^2/gL^3$ equation (5) may be rewritten as

$$(\mathbf{U} \cdot \nabla)\mathbf{U} = -\nabla P + Pr \nabla^2 \mathbf{U} - Ra Pr \theta (\mathbf{e}_g - \gamma (\mathbf{U} \cdot \nabla)\mathbf{U}). \quad (6)$$

As can be seen, equation (6) is consistent with the momentum equation under the Boussinesq approximation, except for the additional inertial buoyancy term on the right hand side. When expressed in this form, it is apparent that the action of this additional term is to modify the effective direction (and strength) of gravity locally throughout the flow. Indeed, regions which are experiencing higher spatial accelerations will experience deviations from the Boussinesq buoyancy approximation. The strength of these deviations relative to gravity is described by the γ parameter.

Once the values of the thermo-fluid parameters in the physical domain are obtained, the Nusselt number is determined. The local and average Nusselt numbers along the walls of the annulus cavity are obtained from

$$Nu_{loc} = -\partial\theta/\partial\tilde{r}|_{wall} \quad (7)$$

and

$$Nu_{ave} = \frac{1}{2\pi(r_i + r_o)} \left[\int_0^{2\pi r_o} Nu_{loc_o} ds + \int_0^{2\pi r_i} Nu_{loc_i} ds \right]. \quad (8)$$

Description of the problem

In this study the proposed model for the non-Boussinesq approximation is applied on the geometry of a concentric horizontal annulus cavity as portrayed in Fig. 1. Boundary conditions are shown in figure 1. The inner and outer radii of the annulus are denoted by r_i and r_o , respectively, with aspect ratio of $\eta = r_o/r_i = 2.6$. The gap between the two cylinders is filled with a fluid with $Pr=7.02$ consistent with water. The inner and outer cylinders are kept at constant temperatures T_h and T_c , respectively ($T_h > T_c$). The reference length, L_{ref} , is equal to the radial gap between cylinders, i.e. $r_o - r_i$. Simulations are carried out for different Rayleigh numbers ranging from 10^1 to 10^5 . A mesh dependency test is conducted and it is found that a uniform 181×181 computational grid achieves numerical convergence to six significant figures.

For the numerical solution of the governing equations, an element-based finite volume method is developed that uses the SIMPLEC algorithm [10] and co-located variables. The problem is 2-D and steady. Coupling between pressure and velocity fields is established via Rhie and Chow interpolation [11]. Accurate performance of the developed solver has already been validated in refs. [12-16].

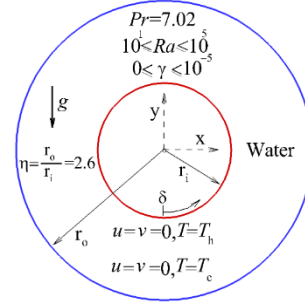


Figure 1. Schematic view and boundary conditions of concentric annulus of two circular cylinders.

Results and discussion

In this section, the results of applying the classic Boussinesq approximation and the non-Boussinesq approximation are presented. Throughout this study, γ is altered between zero and 10^{-5} ($0 \leq \gamma \leq 10^{-5}$). This range is chosen on physical grounds. Under practical applications γ is very small. For instance, taking water at sea level, $\alpha = 1.43 \times 10^{-7} \text{ m}^2/\text{s}$ and $g = 9.81 \text{ m/s}^2$. Hence, over the laboratory scales ranging from $L \sim O(10^{-3} \text{ m})$ to $O(1 \text{ m})$, the parameter ranges from $\gamma = 2 \times 10^{-6}$ down to $\gamma = 2 \times 10^{-15}$. Before presenting the results, for a better understanding of the flows produced in this system, two obtained temperature fields and stream-functions at $Ra=10^5$ with $\gamma = 0$ and $\gamma = 10^{-5}$ are portrayed in figure 2. As can be seen, obtained results from the two approaches are not identical, especially in the temperature field around $\delta = 135^\circ$ and the thickness of the thermal boundary layer at the inner cylinder, and the breadth of the vertical plume. Also for stream-function, aside from different obtained patterns, the maximum value of this parameter and its location, which are shown by a plus sign in two states, are not identical.

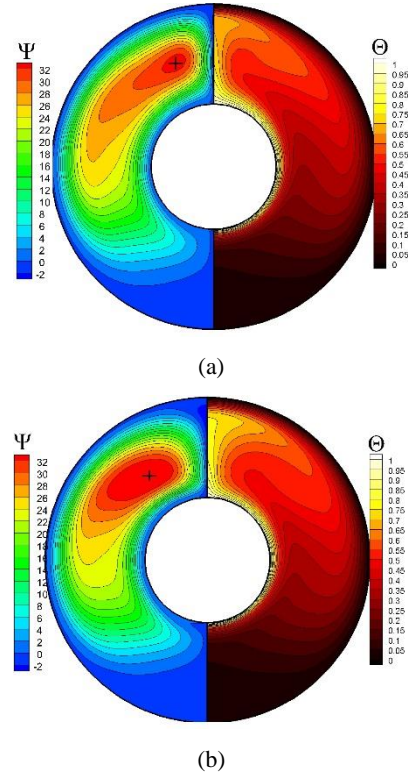


Figure 2. A qualitative comparison between temperature fields and stream-function at $Pr=7.02$ and $Ra=10^5$ (a) $\gamma = 0$ (b) $\gamma = 10^{-5}$.

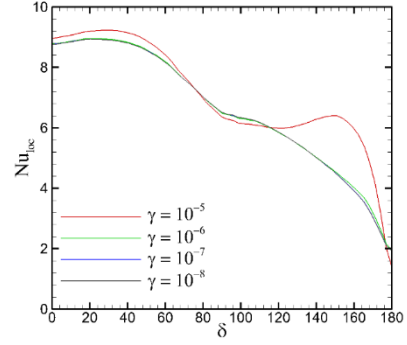
Local Nusselt number

The local Nusselt number distribution along the inner and outer cylinders are plotted in figure 3. Because of symmetry, only half of the local Nusselt number distribution is shown ($0^\circ \leq \delta \leq 180^\circ$). It was found that the local Nusselt number distribution along both surface does not change for $\gamma \leq 10^{-8}$ across the investigated range of Rayleigh number. Thus, for clarity, only the results from $10^{-8} \leq \gamma \leq 10^{-5}$ are presented. For the inner cylinder, the local Nusselt number decreases from $\delta = 0^\circ$ to $\delta = 180^\circ$ (figure 3a). As it can be seen, at $Ra=10^5$, there is a considerable mismatch between computed local Nusselt number at $\gamma = 10^{-5}$ compared to lower values of γ throughout the range of angular positions. Specifically, at $Ra=10^5$ and $\gamma = 10^{-5}$, aside from $80^\circ \leq \delta \leq 130^\circ$, the local Nusselt number distribution along the inner surface has a larger value compared to the lower γ . A visible thinner thermal boundary layer along the inner cylinder in Fig. 2b compared to Fig. 2a after $\delta \cong 130^\circ$ justifies larger value of the local the Nusselt number.

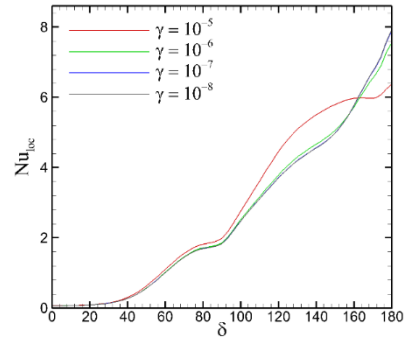
For the outer cylinder (figure 3b), the local Nusselt number increases from $\delta = 0^\circ$ to $\delta = 180^\circ$. Over the lower half of the cylinder ($0 \leq \delta \leq 90^\circ$) there is little difference between each γ value. Beyond $\delta \cong 90^\circ$, the $\gamma = 10^{-5}$ case begins to deviate from lower- γ cases. Along this surface, distribution of the local Nusselt number has a larger value compared to the lower γ value up to $\delta \approx 160^\circ$. The more spread plume that is accompanied with thinner thermal boundary layer in Fig.3b compared to Fig.3a explains the larger value of the local Nusselt number along the outer cylinder up to $\delta \approx 160^\circ$. Note that for both surfaces at $Ra=10^5$, the computed local Nusselt number distributions having $\gamma \leq 10^{-7}$ are almost identical. In other words, the results of $\gamma \leq 10^{-7}$ (non-Boussinesq approximation) and $\gamma = 0$ (Boussinesq approximation) yield the same results at $Ra=10^5$. This is also true for lower Rayleigh numbers ($Ra \leq 10^4$) and the investigated range of γ (figure 3c & figure 3d). Indeed, for $Ra \leq 10^4$, the Boussinesq approximation ($\gamma = 0$) and non-Boussinesq approximation ($\gamma \neq 0$) yield almost identical results. Hence, the results of $Ra=10^2$ are not presented here.

Average Nusselt number

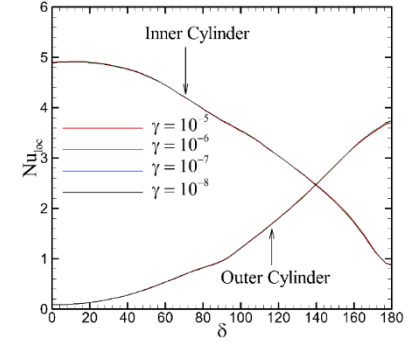
The variation in average Nusselt number with Rayleigh number ($10^1 \leq Ra \leq 10^5$) for $10^{-6} \leq \gamma \leq 10^{-5}$ is plotted in figure 4. In order to evaluate Eq. (8), Simpson's 1/3rd rule of integration is used. As predicted, the average Nusselt number is increased by increasing the Rayleigh number. Across the computed range of Rayleigh number, obtained results for $\gamma \leq 10^{-8}$ are consistent up to six significant figures. Because of close results for $\gamma \leq 10^{-6}$, the computed average Nusselt numbers are plotted only for $10^{-6} \leq \gamma \leq 10^{-5}$ for clarity purposes. Figure 4 indicates that, by increasing the Rayleigh number, the results of Boussinesq and non Boussinesq approximations start to deviate from each other at around $Ra = 6 \times 10^4$. An exact comparison of the average Nusselt number at $Ra = 6.31 \times 10^4$ for $\gamma = 10^{-5}$ and $\gamma = 0$, shows 2.8% mismatch between two approaches. Also, a comparison of the average Nusselt number for the toughest case at $Ra = 10^5$ for the non-Boussinesq with $\gamma = 10^{-5}$ and the Boussinesq case ($\gamma = 0$), yields a 7.38% difference between the two approaches. The corresponding difference in average Nusselt numbers for $Ra \leq 10^4$ is negligible (i.e. $< 0.13\%$). The slight increase in average Nusselt number at the highest Rayleigh number and γ values may be attributed to the tendency of the non-Boussinesq effect to produce thinner boundary layers on the inner cylinder.



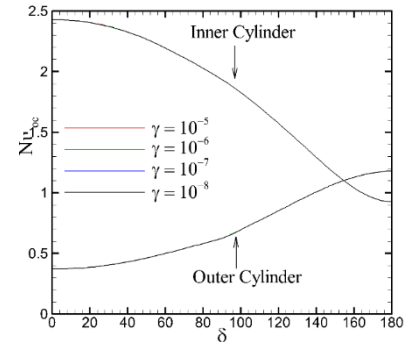
(a) $Ra=10^5$, inner cylinder



(b) $Ra=10^5$, outer cylinder



(c) $Ra=10^4$



(d) $Ra=10^3$

Figure 3. Local Nusselt number distribution along the cylinders with different γ values at different Rayleigh number.

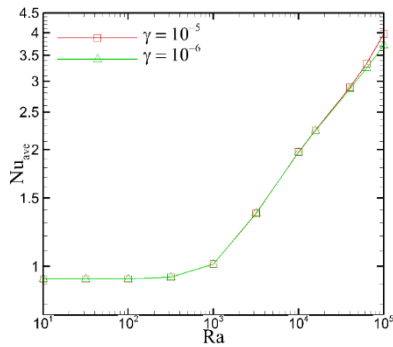


Figure 4. Average Nusselt number versus Rayleigh number for different γ values.

Conclusions

In this study, a non-Boussinesq approximation formulation is proposed for natural convection problems. A dimensionless parameter, the square of the ratio of thermal diffusivity to gravitational effects, $\gamma = \alpha^2/gL^3$, is introduced characterising deviation from the classic Boussinesq approximation at $\gamma = 0$. The proposed formulation is applied to the natural convection in a concentric horizontal annulus cavity with aspect ratio of 2.6 ($r_o/r_i = 2.6$) and results are compared in terms of the local and average Nusselt numbers. Results show that the Boussinesq approximation works accurately up to $Ra=10^4$ but at $Ra=10^5$, distribution of the local Nusselt number is different at larger values of γ . At $Ra=10^5$, a 7.38% difference is observed for average Nusselt number, between the classic Boussinesq approximation ($\gamma = 0$) and the presented non-Boussinesq approximation ($\gamma = 10^{-5}$). It would therefore be expected that non-Boussinesq effects would be likely to be significant at higher Rayleigh numbers, small-scales systems, or for fluids having large thermal expansion coefficients. For example, ammonia and R-12 refrigerant dichlorodifluoromethane have $\alpha \approx 2.5 \times 10^{-3} K^{-1}$ compared to water ($2.14 \times 10^{-4} K^{-1}$), yielding γ more than two orders of magnitude greater at the same scale.

Acknowledgments

This research was supported by the Australian Research Council through Discovery Projects DP150102920 and DP180102647. P. Mayeli is supported by a Monash Graduate Scholarship and a Monash International Postgraduate Research Scholarship. The authors are also supported by a time allocation on the National Computational Infrastructure (NCI) peak facility through an NCMAS grant. NCI is supported by the Australian Government.

References

- [1] Boussinesq, J., *Theorie Analytique de la Chaleur*, Gauthier-Villars, vol. II, 1903.
- [2] Kuhen, T. H. & Goldstein, R. J., An experimental and theoretical study of natural convection in the annulus between horizontal concentric cylinders, *Journal of Fluid Mechanics* **74**, 1976, 695-719. F.
- [3] Abu-Nada, E., Masoud, Z. & Hijazi, A., Natural convection heat transfer enhancement in horizontal concentric annuli using nanofluids, *International Communications in Heat and Mass Transfer* **35**, 2008, 657-665.
- [4] Ashrafizadeh, A. & Nikfar, M., On the numerical solution of generalized convection heat transfer problems via the method of proper closure equations–part II: Application to test problems, *Numerical Heat Transfer Part B* **70**, 2016, 204-222.
- [5] Ashorynejad, H. R., Mohamad, A. A. & Sheikholeslami, M., Magnetic field effects on natural convection flow of a nanofluid in a horizontal cylindrical annulus using Lattice Boltzmann method, *International Journal of Thermal Sciences* **64**, 2013, 240-250.
- [6] Najafi, M. & Enjilela, V., Natural convection heat transfer at high Rayleigh numbers – Extended meshless local Petrov–Galerkin (MLPG) primitive variable method, *Engineering Analysis with Boundary Elements* **44**, 2014, 170-184.
- [7] Szewc, K., Pozorski, J. & Tanière, A., Modelling of natural convection with Smoothed Particle Hydrodynamics: Non-Boussinesq formulation, *International Journal of Heat and Mass Transfer* **54**, 2011, 4807-4816.
- [8] Vierendeels, J., B. Merci, E. Dick, A multigrid method for natural convective heat transfer with large temperature differences, *Journal of Computational and Applied Mathematics* **168**, 2004, 509-517.
- [9] J. M. Lopez, F. Marques, M. Avila, The Boussinesq approximation in rapidly rotating flows, *Journal of Fluid Mechanics* **737** (2013) 56-77.
- [10] J. P. Van Doormal, G. D. Raithby, Enhancement of the SIMPLE method for predicting incompressible fluid flows, *Numerical Heat Transfer* **7** (1984) 147-163.
- [11] Rhie, C. M., Chow, W. L., Numerical study of the turbulent flow past an airfoil with trailing edge separation, *AIAA journal* **21**, 1983, 1525-1532.
- [12] Mayeli, P., Nili-Ahmadabadi, M., Pirzadeh, M.R. & Rahmani, P., Determination of desired geometry by a novel extension of ball spine algorithm inverse method to conjugate heat transfer problems, *Computers & Fluids* **154**, 2017, 390-406.
- [13] Hesami, H. & Mayeli, P., Development of the ball-spine algorithm for the shape optimization of ducts containing nanofluid, *Numerical Heat Transfer Part A* **70**, 2016 1371-1389.
- [14] Nikfar, M. & Mayeli, P., Surface shape design in different convection heat transfer problems via a novel coupled algorithm, *ASME: Journal of heat transfer* **140**, 2018, 021702-1:15.
- [15] Mayeli, P., Hesami, H., Moghaddam, M. H. D. F., Numerical investigation of the MHD forced convection and entropy generation in a straight duct with sinusoidal walls containing water-Al₂O₃ nanofluid, *Numerical Heat Transfer Part A* **71**, 2017, 1371-1389.
- [16] Mayeli, P., Hesami, H., Besharati-Foumani, H. & Nijalili, M., Al₂O₃–Water nanofluid heat transfer and entropy generation in a ribbed channel with wavy wall in the presence of magnetic field, *Numerical Heat Transfer Part A* **73**, 2018, 604-623.